Acta Materialia 125 (2017) 390–400

Contents lists available at ScienceDirect

Acta Materialia

journal homepage: www.elsevier.com/locate/actamat

Full length article

In situ tailoring microstructure in additively manufactured Ti-6Al-4V for superior mechanical performance

W. Xu [a, b, *], E.W. Lui [b], A. Pateras [b], M. Qian [b], M. Brandt [b, **]

[a] Department of Engineering, Macquarie University, New South Wales 2109, Australia
[b] Centre for Additive Manufacturing, School of Engineering, RMIT University, Melbourne, VIC 3000, Australia

ARTICLE INFO

Article history:
Received 1 November 2016
Received in revised form
12 December 2016
Accepted 13 December 2016
Available online 19 December 2016

Keywords:
Ti-6Al-4V
Selective laser melting
Additive manufacturing
Microstructural control
Martensite decomposition

ABSTRACT

The "Holy Grail" of metal additive manufacturing is to manufacture reliable high-performance metal parts with no or a minimal need of post processing. However, Ti-6Al-4V parts made by selective laser melting (SLM) often suffer from poor ductility and low toughness because of the predominant acicular α′ martensite contained in columnar prior-β grains. In practice, post heat treatment is necessary. To overcome this deficiency, we have explored designing innovative SLM processing routes to turn the unfavoured α′ martensite, via *in-situ* decomposition, into lamellar (α+β) microstructures with tuneable characteristic length scales. Such lamellar (α+β) microstructures lead to superior mechanical properties which markedly exceed ASTM standards and outperform the majority of Ti-6Al-4V fabricated by other additive manufacturing processes. Furthermore, we find that the lattice parameter of the β phase in the (α+β) lamellae falls into a specific range of 3.18–3.21 Å. Hence the lattice parameter of β phase can serve as an indicator to predict whether significant martensite decomposition has taken place *in situ* in Ti-6Al-4V made by SLM. This work marks an important step forward in the understanding of how to tailor microstructure *in situ* for the development of high-performance Ti-6Al-4V parts by SLM.

© 2016 Acta Materialia Inc. Published by Elsevier Ltd. All rights reserved.

1. Introduction

Microstructure is a fingerprint for the prediction of macroscopic mechanical behaviour for most materials. For conventional metal casting and forming practices, controlling microstructure by suitable process control is commonly used to produce materials with desired mechanical performance. In the case of powder-bed fusion (PBF) metal additive manufacturing (AM) or 3D printing, precise microstructural control, however, is not easily achievable as the energy beam-powder interaction is highly dynamic and the thermal history associated with PBF-AM processes is very complex [1,2]. This has also proved to be challenging for achieving high-performance Ti-6Al-4V (the "workhorse" alloy in the titanium industry) by SLM, which is the most broadly used PBF process. In general, additively manufactured Ti-6Al-4V by SLM is stronger (in terms of strength) than its wrought counterparts, but for structural applications its tensile ductility and toughness need to be substantially improved [3–8]. The inadequate ductility is caused by the presence of undesired α′ martensites in columnar prior-β grains because of their low capacity to tolerate crack initiation and propagation [8–13]. Consequently, post-SLM heat treatment is often necessary but that affects the effectiveness of the AM process.

A major challenge is therefore to replace martensite by favoured α and β phases naturally during SLM processing in a controllable manner. More importantly, being able to turn α′ martensite *in situ* into a series of lamellar (α+β) microstructures with tuneable length scales will enable the achievement of various combinations of strength and ductility while minimizing the need for post processing. Recently, we have suggested that the use of an array of properly selected SLM processing variables (e.g. focal offset distance, *FOD*, and energy density, *E*) is able to transform the acicular α′ martensite *in situ* into lamellar (α+β) in the as-built Ti-6Al-4V [8,14]. The resulting α laths were about 0.2–0.3 μm thick, and such an ultrafine microstructure led to superior tensile properties in the as-built state (yield strength of 1106 ± 6 MPa and total elongation to failure of 11.4 ± 0.4%) [8,14]. However, owing to the limited processing window of adjusting *FOD* and the high sensitivity of microstructure to *FOD*, it is less practical, without post heat treatment, to achieve a broad range of desired microstructures for

* Corresponding author. Department of Engineering, Macquarie University, New South Wales 2109, Australia.
** Corresponding author.
E-mail addresses: wei.xu@mq.edu.au (W. Xu), milan.brandt@rmit.edu.au (M. Brandt).

http://dx.doi.org/10.1016/j.actamat.2016.12.027
1359-6454/© 2016 Acta Materialia Inc. Published by Elsevier Ltd. All rights reserved.

Table 1
Summary of SLM processing variables used in this study.

Variables	A_S/A_P	D (mm)	t_i (s)	t (μm)	FOD (mm)	P (W)	V (mm s^{-1})	h (mm)	E (J mm^{-3})
Support structure (Group 1)	0.125	12	1	60	2	375	1029	0.12	50.62
	0.25	12	1	60	2	375	1029	0.12	50.62
	0.4	12	1	60	2	375	1029	0.12	50.62
	1.0	12	1	60	2	375	1029	0.12	50.62
Inter-layer time (Group 2)	0.4	12	1	60	2	375	1029	0.12	50.62
	0.4	12	5	60	2	375	1029	0.12	50.62
	0.4	12	8	60	2	375	1029	0.12	50.62
	0.4	12	10	60	2	375	1029	0.12	50.62
Layer thickness (Group 3)	0.4	12	1	90	2	375	686	0.12	50.62
	0.4	12	8	90	2	375	686	0.12	50.62
	0.4	12	10	90	2	375	686	0.12	50.62
Part dimension (Group 4)	0.4	12	1/5	60	2	375	1029	0.12	50.62
	0.4	5	1/5	60	2	375	1029	0.12	50.62
	0.4	4	1/5	60	2	375	1029	0.12	50.62
	0.4	3	1/5	60	2	375	1029	0.12	50.62
	0.4	2	1/5	60	2	375	1029	0.12	50.62
	0.4	1	1	60	2	375	1029	0.12	50.62
	0.4	0.8	1	60	2	375	1029	0.12	50.62

A_S/A_P – area ratios between support structure and part; D – part diameter; t_i – inter-layer time; t – layer thickness;FOD – focal offset distance; P – laser power; V – scanning velocity; h – hatch spacing; E – energy density.

structural applications in the as-built state.

The key hypothesis behind this study is that the additive nature of the successive layer-by-layer fabrication can be used to control the thermal profile of the preceding solidified layers. α′ martensite is predominant in SLM Ti-6Al-4V under normal SLM conditions. However, with a properly designed SLM process, we assume that the temperature of each preceding solidified layer can be raised *in situ*, as a result of the layer additive nature of the SLM process, to a range (e.g. 600–850 °C) that can effectively encourage α′ martensite decomposition. If the required temperature profile can be maintained sufficiently long, then a complete transformation from α′ martensite into (α+β) is achievable. In addition, the expected temperature rise (from its low operating temperature of 200 °C to 600–850 °C) can lead to a decrease in both cooling rate and temperature gradient thereby improving microstructural anisotropy and reducing residual stress.

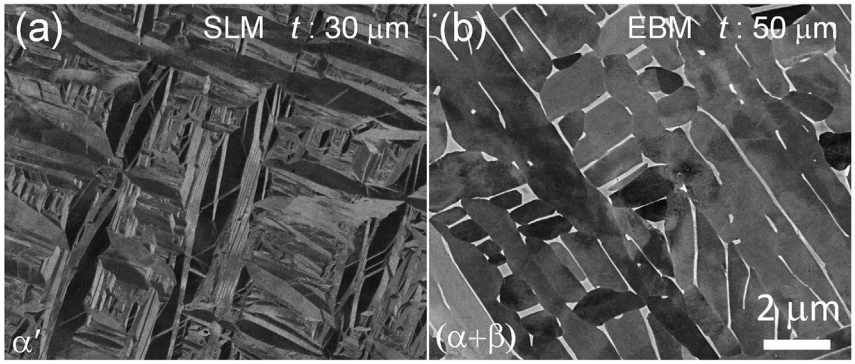

Fig. 1. Typical microstructure commonly achieved in as-fabricated Ti-6Al-4V by additive manufacturing. (a) α′ martensite in SLM as-built Ti-6Al-4V using 30 μm layer thickness and platform temperature of 200 °C. (b) Lamellar (α+β) in EBM as-built Ti-6Al-4V using Arcam A2 with layer thickness of 50 μm and platform temperature of 730 °C [18].

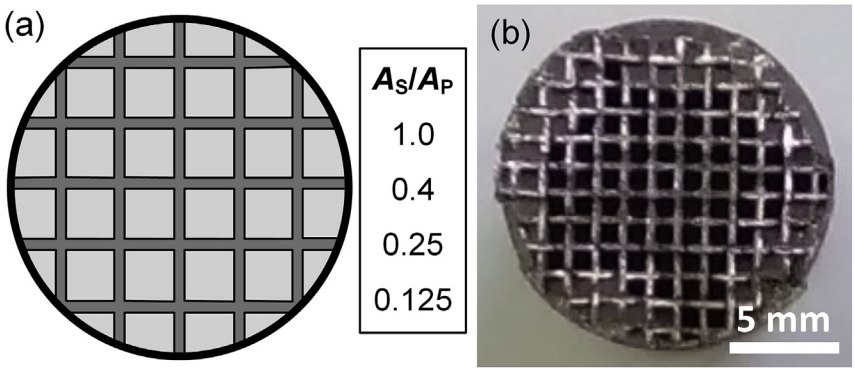

Fig. 2. (a) A schematic diagram of support structure used in this study. (b) A micrograph of a support structure with $A_S/A_P = 0.25$.

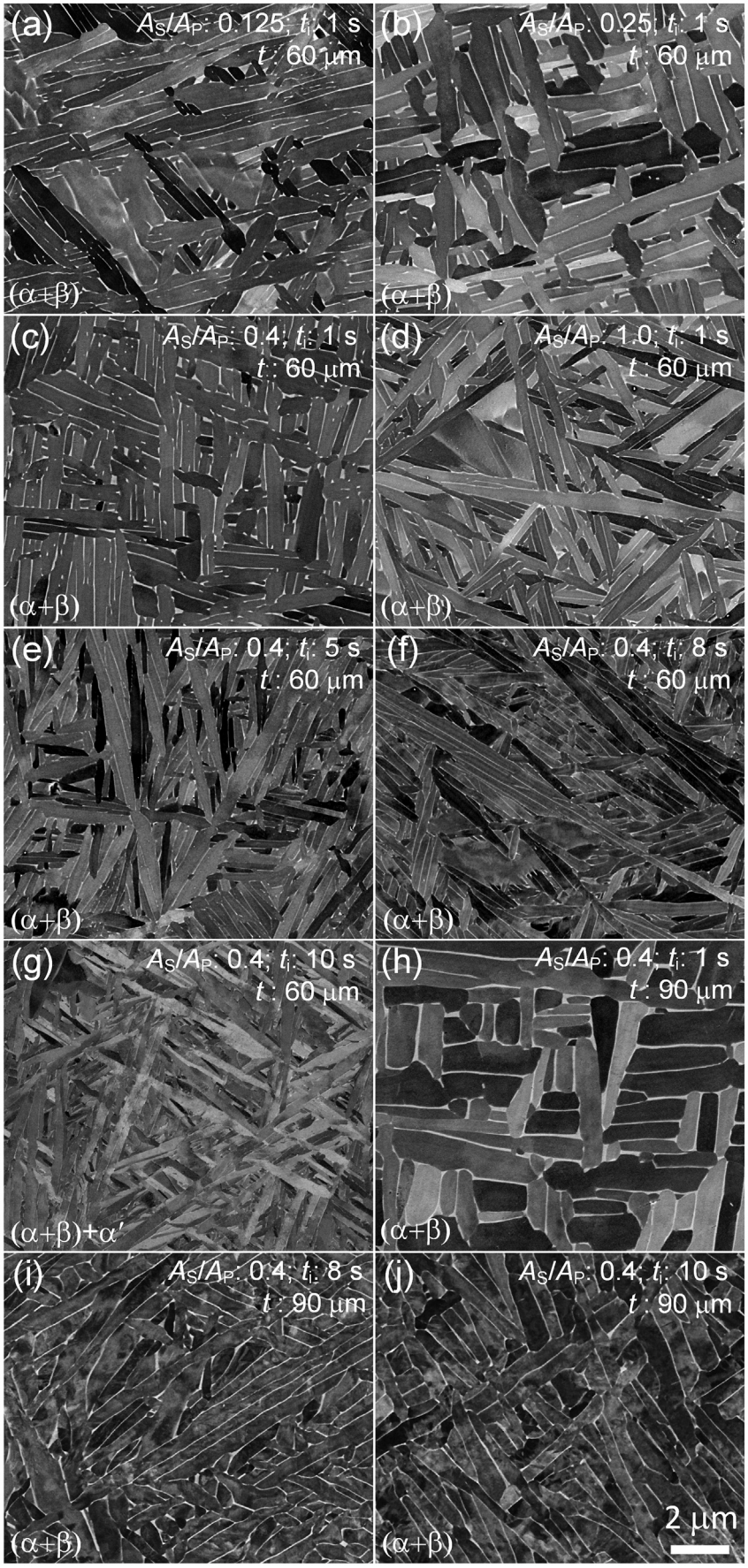

Fig. 3. Microstructure variation in SLM as-built Ti-6Al-4V with diameter of 12 mm. (a) $A_S/A_P = 0.125$, $t_i = 1$ s, $t = 60$ μm. (b) $A_S/A_P = 0.25$, $t_i = 1$ s, $t = 60$ μm. (c) $A_S/A_P = 0.4$, $t_i = 1$ s, $t = 60$ μm. (d) $A_S/A_P = 1.0$, $t_i = 1$ s, $t = 60$ μm. (e) $A_S/A_P = 0.4$, $t_i = 5$ s, $t = 60$ μm. (f) $A_S/A_P = 0.4$, $t_i = 8$ s, $t = 60$ μm. (g) $A_S/A_P = 0.4$, $t_i = 10$ s, $t = 60$ μm. (h) $A_S/A_P = 0.4$, $t_i = 1$ s, $t = 90$ μm. (i) $A_S/A_P = 0.4$, $t_i = 8$ s, $t = 90$ μm. (j) $A_S/A_P = 0.4$, $t_i = 1\ 0$ s, $t = 90$ μm.

Presented here are our latest research findings on microstructural control of additively manufactured Ti-6Al-4V by SLM. We show that, by designing innovative SLM processing routes, it is practical to attain significant *in-situ* α′ martensite decomposition to produce lamellar (α+β) microstructures with a tuneable α lath width ranging from 0.15 μm to 0.8 μm. Another distinct benefit arising from the innovative SLM processing routes is the transition from columnar to equiaxed prior-β grains. Consequently, an excellent combination of strength (yield strength: 1020–1110 MPa) and ductility (total elongation to failure: 11–15%) was achieved in SLM Ti-6Al-4V in the as-built state. Furthermore, significant *in situ* martensite decomposition also leads to a reduction of residual stress, which will be addressed elsewhere together with results of post heat treatment.

2. Experimental procedures

Spherical gas atomized Ti-6Al-4V powder (25–45 μm, ASTM Grade 23, ELI, 0.1% O, 0.009% N, 0.008% C, 0.17% Fe, <0.002% H, TLS Technik GmbH & Co.) was used for SLM processing in this study. A series of cylindrical rods with a diameter of 0.8–12 mm and a height of 30 mm were vertically fabricated using SLM 250 HL (SLM Solutions GmbH; flow Ar; oxygen level < 0.1%; chamber temperature, 200 °C). Table 1 presents the SLM processing variables used in this study to understand the role of support structure (Group 1), inter-layer time (Group 2), layer thickness (Group 3) and part dimension (Group 4) in microstructure control. All samples were produced by using a chessboard scanning strategy.

For microscopic studies, longitudinal and transverse sections of the as-fabricated Ti-6Al-4V were prepared by conventional mechanical grinding and polishing (without chemical etching). Microstructure analysis was performed using FEI's extreme high-resolution scanning electron microscopy (SEM, FEI Verios 460L) and transmission electron microscopy (TEM, JEOL 2100F, 200 kV) equipped with high-angle annular dark field detector (HAADF, scanning TEM mode, STEM) and energy dispersive X-ray spectrometer (EDS). STEM/EDS was used for elemental analysis of α and β phases by means of mapping, line scan and single spectrum (point). Samples for TEM analysis were prepared by the conventional method of slicing and grinding, followed by Ar ion milling (Gatan 691 PIPS). Data for phase identification were acquired using X-ray diffractometry (XRD, Bruker D8, Cu Kα) and analysed using the MAUD program. Quantitative image analysis was conducted using ImageJ for the measurement of the width of α and β laths.

Cylindrical Ti-6Al-4V rods (diameter: 12 mm; height: 100 mm) were fabricated using SLM and then machined into dog-bone shaped tensile specimens with a gauge diameter of 6 mm, gauge length of 24 mm, and length of reduced section of 30 mm (ASTM Standard E8/E8M-09). Quasi-static uniaxial tensile testing with an initial strain rate of $2.5 \times 10^{-4} s^{-1}$ was performed at room temperature on three specimens per processing condition using an MTS universal testing facility (MTS 810, 100 kN) equipped with a non-contact laser extensometer.

3. Results and discussion

3.1. Role of some SLM variables in microstructural control of Ti-6Al-4V

Owing to rapid cooling (10^3–10^5 K/s) and high temperature gradient (10^4–10^5 K/cm) in the melt pool [15,16], the salient feature of the microstructure in SLM Ti-6Al-4V is acicular α′ martensite (Fig. 1a) contained within columnar prior-β grains (Fig. 1a–c in Ref. [8]). This is in contrast to Ti-6Al-4V built by electron beam melting (EBM) whose thermal environment is in favour of the lamellar (α+β) microstructure (Fig. 1b) for better ductility and lower residual stress [17,18]. To challenge such an unfavoured microstructure, one needs to dramatically reduce cooling rate and temperature gradient. Without raising platform temperature to above 600 °C (like the case for EBM), optimising SLM process variables becomes the only feasible option to promote *in-situ* transformation from α′ martensite into (α+β). Our recent progress [8,14] has corroborated that this approach is practically feasible via a proper selection of focal offset distance and energy density. The major drawback of *FOD* is its limited adjustable range in favour of α′ martensite decomposition. Here we introduce several SLM variables which play important roles in microstructural control of Ti-6Al-4V but are often readily overlooked by the majority of studies.

3.1.1. Support structure

Support structures with a variety of area ratios between support structure and part (A_S/A_P: 0.125–1.0, Fig. 2) were used to clarify their effect on microstructure achieved in SLM Ti-6Al-4V. $A_S/A_P = 1.0$ represents the case that the part is directly built onto the platform without support structure, whereas $A_S/A_P = 0.125$ has the least contact area between the support structure and the part. Under the selected processing conditions (Group 1 in Table 1), a full lamellar (α+β) microstructure (Fig. 3a–d) was achieved in all parts irrespective of A_S/A_P. The increase in A_S/A_P from 0.125 to 1.0 led to finer lamellar microstructure, indicative of more significant *in-situ* decomposition favoured in the case of smaller support/part contact area. The width of α lath in the lamellar microstructure increased from 0.30 ± 0.11 μm to 0.59 ± 0.21 μm while reducing A_S/A_P from 1.0 to 0.125 (Fig. 4a). This dependency of microstructure on A_S/A_P implies that thermal environment of the overhanging sections or the vicinity of pores in a part is in favour of *in-situ* α′ martensite decomposition.

3.1.2. Inter-layer time

Fig. 3c, e–g shows the variation in microstructure as a function of inter-layer time (t_i = 1, 5, 8, 10 s; Group 2 in Table 1). For the

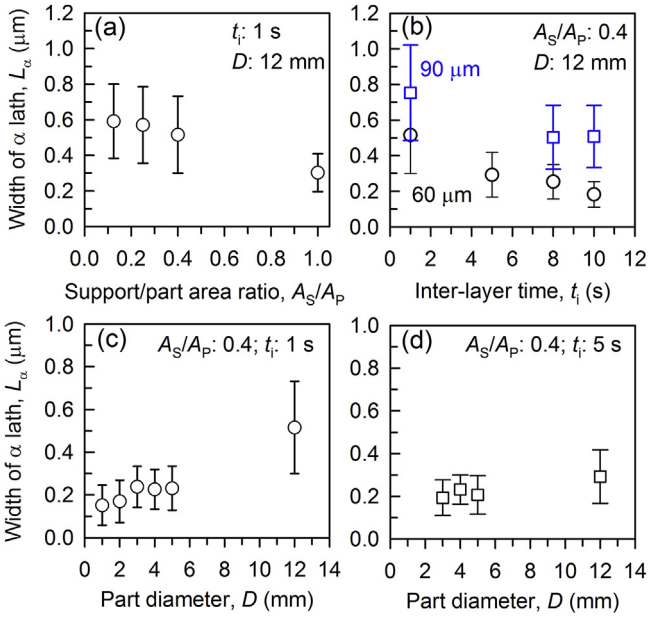

Fig. 4. Width of α laths (L_α) of the lamellar (α+β) in SLM as-built Ti-6Al-4V. (a) L_α dependency on support/part area ratio, t_i = 1 s, D = 12 mm, t = 60 μm. (b) L_α dependency on inter-layer time and layer thickness, A_S/A_P = 0.4, D = 12 mm. (c) L_α dependency on part dimension, A_S/A_P = 0.4, t_i = 1 s. (d) L_α dependency on part dimension, A_S/A_P = 0.4, t_i = 5 s.

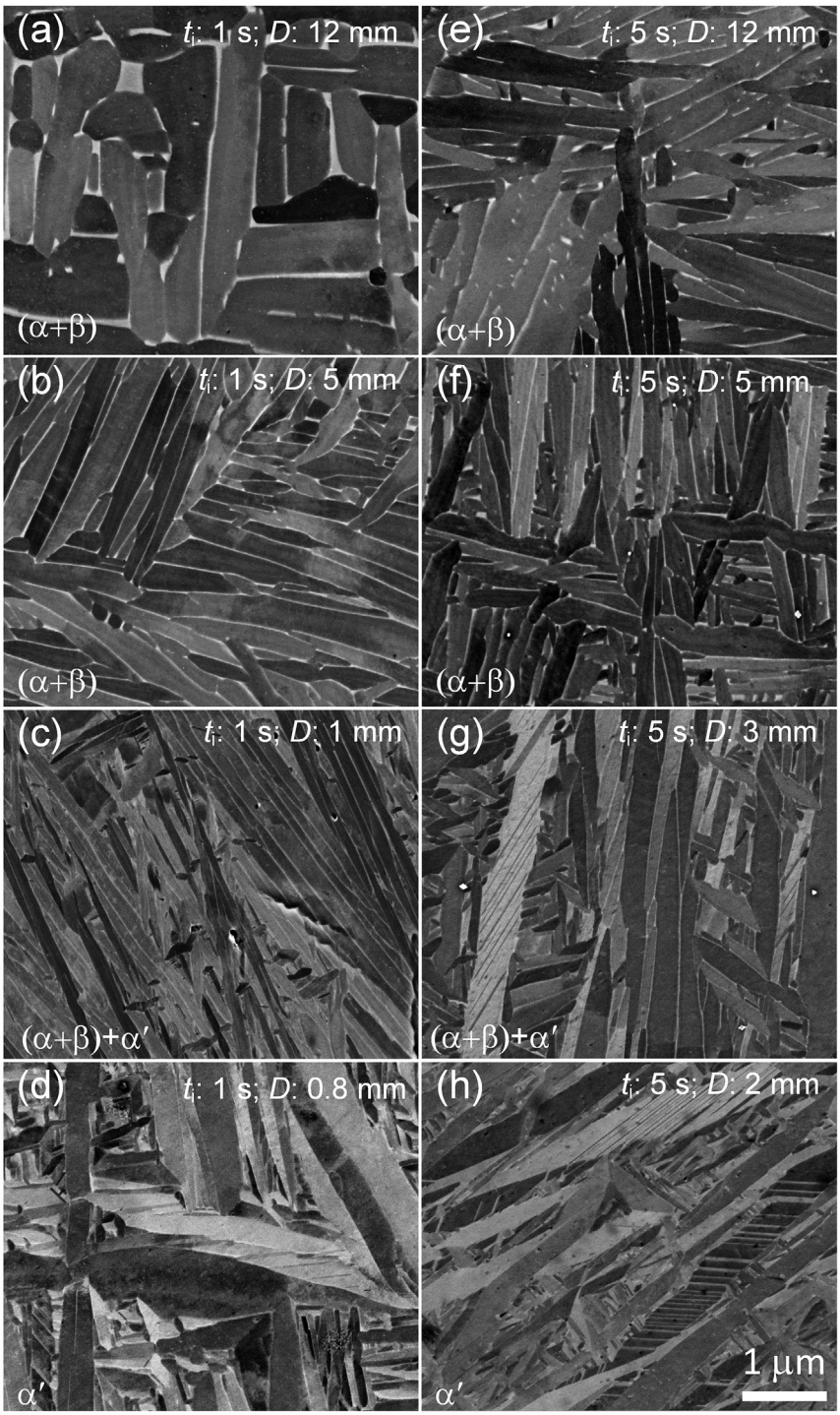

Fig. 5. Effect of part dimension on microstructure in SLM Ti-6Al-4V fabricated using layer thickness of 60 μm and $A_S/A_P = 0.4$. (a) $t_i = 1$ s, $D = 12$ mm. (b) $t_i = 1$ s, $D = 5$ mm. (c) $t_i = 1$ s, $D = 1$ mm. (d) $t_i = 1$ s, $D = 0.8$ mm. (e) $t_i = 5$ s, $D = 12$ mm. (f) $t_i = 5$ s, $D = 5$ mm. (g) $t_i = 5$ s, $D = 3$ mm. (h) $t_i = 5$ s, $D = 2$ mm.

shortest inter-layer time of 1 s, a relatively coarse lamellar (α+β) microstructure (Fig. 3c) was produced as a result of extensive *in-situ* martensite decomposition. Increasing t_i led to refined lamellar microstructure in the case of 5 s (Fig. 3e) and 8 s (Fig. 3f), and a microstructure comprised of mixed lamellar (α+β) and α′ martensite while using 10 s (Fig. 3g). The retained α′ martensite is direct evidence of limited/incomplete *in-situ* decomposition. This indicates that longer inter-layer time is not beneficial to achieve the lamellar (α+β) microstructure. The width of α lath in the lamellar microstructure was strongly influenced by the inter-layer time. With an increase in t_i from 1 s to 10 s, the width of α lath substantially decreased from 0.52 ± 0.22 μm to 0.18 ± 0.07 μm (Fig. 4b). Compared to support structure, it is clear that the inter-layer time is a more influential and decisive factor in promoting *in-situ* martensite decomposition for the achievement of a lamellar (α+β) microstructure.

3.1.3. Layer thickness

Fig. 3h–j presents the microstructure variation as a function of inter-layer time when a layer thickness of 90 μm is selected (Group

3 in Table 1). Analogous to the layer thickness of 60 μm (Fig. 3c, e–g), increasing inter-layer time also led to finer lamellar (α+β) microstructure in the case of 90 μm. The width of α lath decreased from 0.75 ± 0.27 μm to 0.51 ± 0.18 μm with increasing t_i from 1 s to 10 s (Fig. 4b). Compared with layer thickness of 60 μm, increasing layer thickness to 90 μm resulted in much coarser lamellar (α+β) microstructure, indicative of more significant *in-situ* martensite decomposition. Furthermore, with increasing t_i the decrease in average α lath width is much less in the case of 90 μm layer thickness, implying that *in-situ* martensite decomposition is less sensitive to inter-layer time at larger layer thickness. This enables a broader processing window to achieve the desired lamellar (α+β) microstructure.

3.1.4. Part dimension

To reveal the effect of part dimension, cylindrical rods of diameter ranging from 0.8 mm to 12 mm were produced (Group 4 in Table 1). At a given inter-layer time of 1 s, Fig. 5a–d shows the microstructure variation as a function of part diameter. It is clear that the part with a large diameter of 12 mm presents a coarse lamellar (α+β) microstructure (Fig. 5a) after experiencing extensive *in-situ* martensite decomposition. As the diameter decreased, the (α+β) lamellae became finer (Fig. 5b) until the emergence of retained α′ martensite in the part of 1 mm in diameter. Below 1 mm, α′ martensite was predominant and the overall quantity of detectable β phase was minimal. In the case of inter-layer time of 5 s, the resultant lamellar (α+β) microstructures (Fig. 5e–h) were much finer than that of 1 s. The minimum diameter required to achieve a full lamellar (α+β) microstructure was 4 mm, which is larger than that of 2 mm for 1 s. Below 4 mm, α′ martensite appeared (Fig. 5g) and was largely retained in the 2 mm part due to very limited martensite decomposition (Fig. 5h). Fig. 4c and d presents the variation in α lath width as a function of part diameter. For inter-layer time of 1 s, the α lath width decreased from 0.52 ± 0.22 μm to 0.15 ± 0.09 μm as part diameter decreased from 12 mm to 1 mm (Fig. 4c). On the other hand, for inter-layer time of 5 s the variation of α lath width is marginal (from 0.29 ± 0.13 μm to 0.19 ± 0.08 μm) with decreasing diameter from 12 mm to 3 mm (Fig. 4d). This further corroborates the decisive role of inter-layer time in facilitating *in-situ* martensite decomposition.

3.2. Microstructural signature of lamellar (α+β) in SLM Ti-6Al-4V

The transformation of acicular α′ martensite into lamellar (α+β) is thermally activated and diffusion-controlled [19,20]. The achievable microstructure depends on the transformation temperature and its residence time. As the decomposition of α′ martensite takes place *in situ* during SLM processing, V (β stabilizer) partitions to the β phase and Al (α stabilizer) tends to segregate to the α phase. The β phase is thus enriched in V and depleted in Al, and its lattice parameter is strongly correlated with the content of V. Higher V usually results in smaller lattice parameter in β [21]. Thermodynamically, the V content in β phase is determined by the transformation temperature at which β phase nucleates and grows. Higher temperature leads to lower V content in β phase [22].

Based on the above correlation between transformation temperature, V content and lattice parameter in β phase, it is possible to predict whether significant α′ martensite decomposition takes place during SLM processing and estimate the temperature range leading to such an *in situ* decomposition. Fig. 6a–c presents X-ray diffraction profiles corresponding to microstructures shown in Fig. 3a–j. The appearance of $(110)_\beta$ peak at 39.5° and $(200)_\beta$ peak at 57.5° verified the presence of a certain amount of β phase in those as-built Ti-6Al-4V samples. Fig. 6d compares XRD profiles of several typical microstructures, near full α′ martensite (Fig. 1a), a mixture

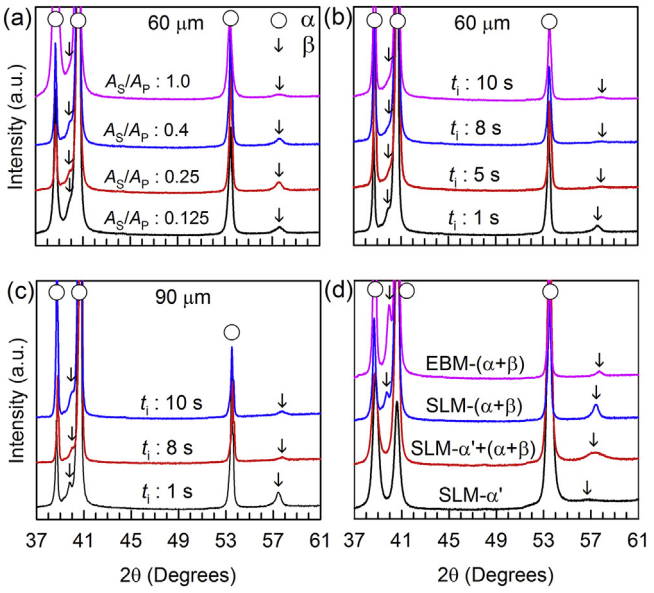

Fig. 6. X-ray diffraction patterns of SLM as-built Ti-6Al-4V. (a) Dependency on support/part area ratio. (b) Dependency on inter-layer time for layer thickness of 60 μm, $A_S/A_P = 0.4$, $D = 12$ mm. (c) Dependency on inter-layer time for layer thickness of 90 μm, $t_i = 1$ s, $D = 12$ mm. (d) Comparison between different microstructures in SLM and EBM as-built Ti-6Al-4V.

of α′ and lamellar (α+β), and full lamellar (α+β) achieved in SLM Ti-6Al-4V (Fig. 3h), and full lamellar (α+β) in EBM Ti-6Al-4V (Fig. 1b). The full lamellar (α+β) microstructures in SLM and EBM Ti-6Al-4V are analogous in morphology (Fig. 3h and 1b) but the later has a slightly larger amount of β phase. For SLM Ti-6Al-4V with near full α′ martensite, even though β phase is hardly revealed from the microstructure (Fig. 1a), a tiny peak close to 56.5° can be detected, indicating the presence of a small amount of β phase. Its β lattice parameter of 3.26 Å is noticeably larger than that in the full lamellar (α+β) microstructure. This implies that the β phase present in SLM Ti-6Al-4V with near full α′ martensite has formed at higher temperature and a lower V content is thus expected.

We summarize, in Fig. 7, c/a ratio of α/α′ vs. β lattice parameter a after fitting the XRD profiles of both SLM and EBM as-built Ti-6Al-4V. Four types of microstructures were present for comparison, near full α′ martensite, a mixture of α′+(α+β) dominated by α′, a mixture of (α+β)+α′ dominated by (α+β), and full lamellar (α+β). There is a clear correlation between resultant microstructures and

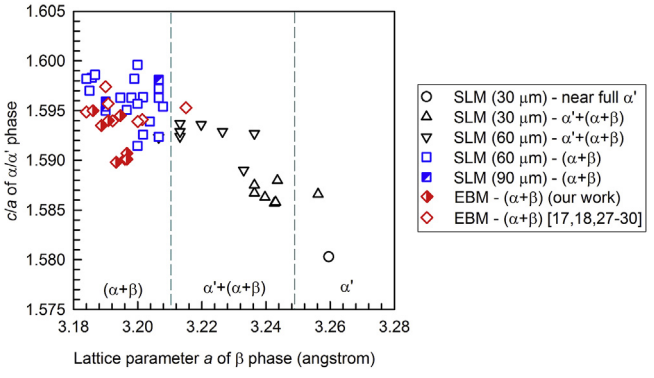

Fig. 7. c/a ratio of α/α′ vs. β lattice parameter a for SLM and EBM as-built Ti-6Al-4V with different microstructures. Data for SLM as-built Ti-6Al-4V and some EBM as-built Ti-6Al-4V were obtained in our work. Some data (open diamond symbol) for EBM as-built Ti-6Al-4V were acquired from Refs. [17,18,27–30].

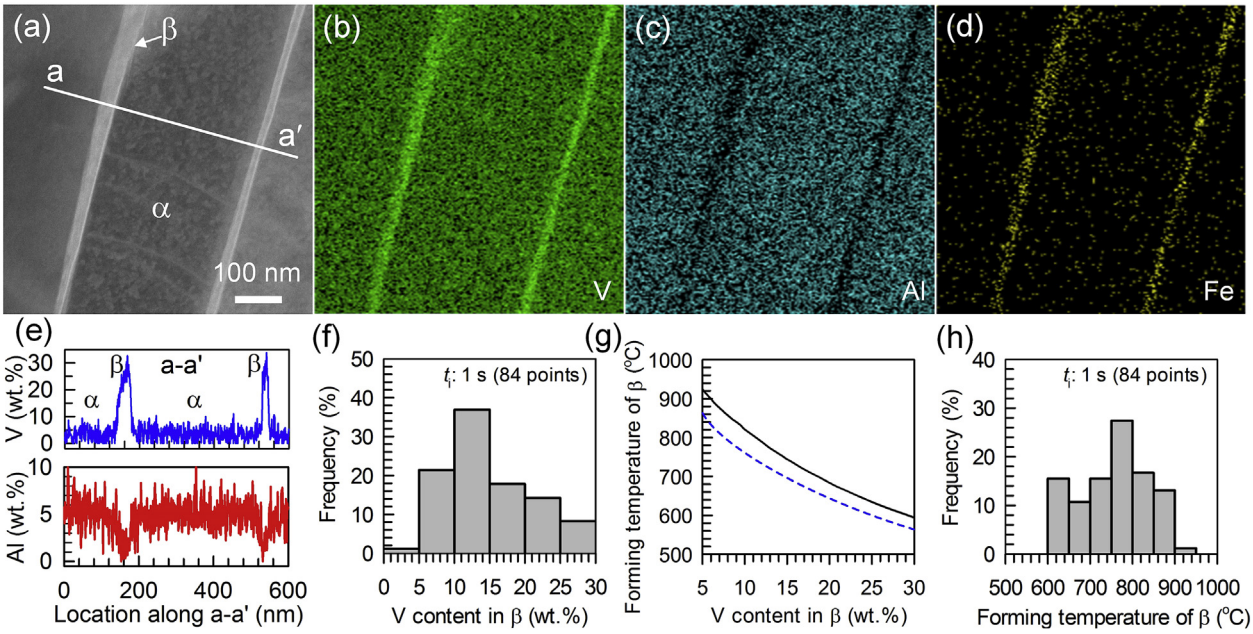

Fig. 8. STEM/EDS mapping, line scanning and point analysis on the lamellar (α+β) microstructure achieved in SLM as-built Ti-6Al-4V (Fig. 3a, $A_S/A_P = 0.125$, $t_i = 1$ s, $t = 60$ μm). (a) STEM image. (b–d) EDS mapping, V, Al, Fe. (e) EDS line scanning along a-a′ in (a). (f) Frequency distribution of V presented in β based on EDS point analysis. (g) Calculated V content of β phase as a function of temperature [22] with dashed line showing a shift for the non-equilibrium case. (h) Frequency distribution of β forming temperature converted from (f).

lattice constants of β and α/α′ phases. In the case of near full α′ martensite with minimum decomposition, the lattice parameter of the detectable β phase is 3.26 Å and the *c*/*a* ratio of α/α′ is 1.580. As decomposition of α′ martensite becomes more significant, the lattice parameter of β phase decreases and the *c*/*a* ratio of α/α′ increases, until reaching a regime where a full lamellar (α+β) microstructure is usually observed. After significant *in-situ* martensite decomposition, the lamellar (α+β) achieved in both SLM and EBM as-built Ti-6Al-4V has exhibited β lattice parameter near 3.18–3.21 Å and *c*/*a* ratio of α close to 1.590–1.600. The lattice parameter of β phase can thus be treated as a microstructural signature so that one can predict whether a lamellar (α+β) microstructure is achieved in SLM as-built Ti-6Al-4V.

3.3. Compositional analysis of lamellar (α+β) in SLM Ti-6Al-4V

To determine the temperature range for the achievement of the full lamellar (α+β), we analysed the composition in α and β phases using STEM/EDS with special attention made to the V content in β phase (Fig. 8). The STEM/EDS mapping (Fig. 8a–d) and line scanning (Fig. 8e) analyses clearly revealed the partitioning of V (up to 30 wt%) and Fe (up to 3.5 wt%) to the β phase. Furthermore, the EDS point analysis on a large number of β laths provided a frequency distribution of V presented in the β phase. In the case shown in Fig. 8f, the V content in β phase varied from 5–10 wt% to 25–30 wt% with the majority of β laths having V in a broad range of 5–25 wt%. The presence of such a large variation in V is the direct consequence of repetitive heating and cooling arising from the layer-wise fabrication. Considering the correlation between V content and β forming temperature (Fig. 8g), we can convert the compositional frequency distribution (Fig. 8f) into a frequency distribution of β forming temperature (Fig. 8h). In reality, because of the rapid heating-cooling nature of SLM processing there is a shift of the V content from its equilibrium in the β phase. Limited by the incomplete diffusion, a lower V content (marked by the dashed line in Fig. 8g) is usually present in β than that of equilibrium value. In this case, the predicted β forming temperature shown in Fig. 8h by the direct conversion from Fig. 8f is higher than the actual temperature. We expect a maximum shift of 30–50 °C toward the lower side. Taking this possible shift into account, we can semi-quantitatively predict a temperature range of 600–850 °C at which the majority of the β laths are formed as a result of significant *in-situ* α′ martensite decomposition. In turn, this indicates that during SLM processing the temperature of the preceding solidified layers is raised to such a range and maintained for a sufficiently long residence time to produce the lamellar (α+β) microstructure. The predicted temperature range is also consistent with that reported for α′ martensite decomposition [19]. Below 600 °C the decomposition is very limited and above 800 °C a complete transformation can be achieved. However, the temperature needs to be controlled below 900 °C because above it α′ martensite reforms upon rapid cooling [21].

Another characteristic length scale requiring special attention is the width of β laths, which is directly associated with the diffusion of V. The β lath width measured from the STEM images is presented as a function of inter-layer time (Fig. 9a) and support/part area ratio (Fig. 9b). Shorter t_i and smaller A_S/A_P produced coarser β laths. For instance, in the case shown in Fig. 9a the width of β laths decreased

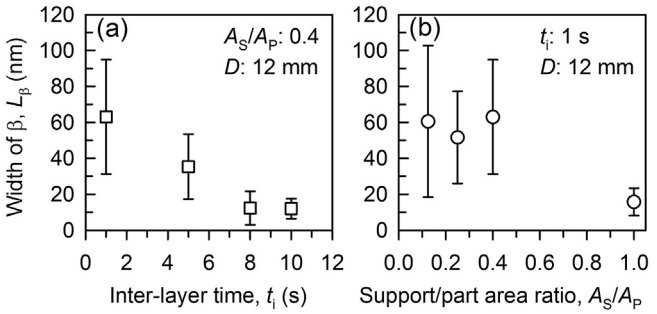

Fig. 9. Dependency of β lath width (L_β) on (a) inter-layer time, $A_S/A_P = 0.4$, $D = 12$ mm, $t = 60$ μm and (b) support/part area ratio, $t_i = 1$ s, $D = 12$ mm, $t = 60$ μm.

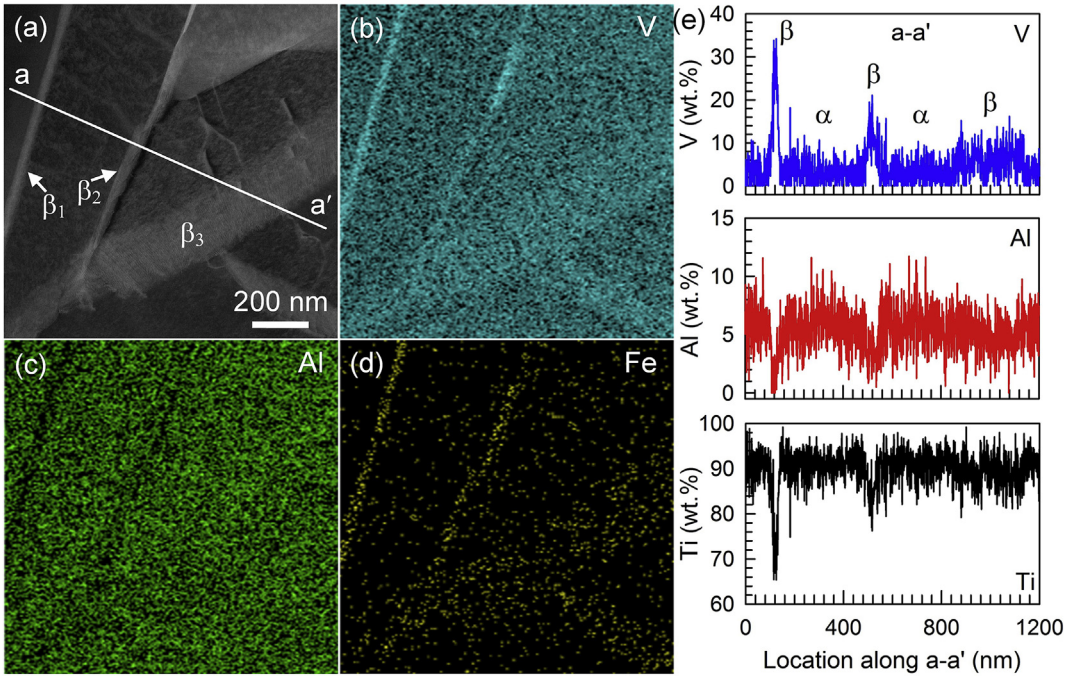

Fig. 10. STEM/EDS analysis on the lamellar (α+β) microstructure achieved in SLM as-built Ti-6Al-4V (Fig. 3a, $A_S/A_P = 0.125$, $t_i = 1$ s, $t = 60$ μm), showing that finer β laths have higher V content. (a) STEM image. (b–d) EDS mapping, V, Al, Fe. (e) EDS line scanning along a-a′ in (a).

from 63 ± 32 nm to 12 ± 6 nm with increasing t_i from 1 s to 10 s. This is analogous to the trend for α laths (Fig. 4a and b) and is another evidence to support our earlier claim that shorter t_i and smaller A_S/A_P promote *in-situ* martensite decomposition. Further looking into this phenomenon, a shorter inter-layer time leads to a shorter overall duration of processing. To produce coarser α and β laths, a sufficiently high temperature (but below 900 °C) needs to be quickly reached for significant martensite decomposition. This is consistent with the thermal environment of shorter t_i and smaller A_S/A_P under which the limited heat dissipation facilitates a rapid temperature rise due to heat build-up. As the width of β laths is correlated with diffusion length of V, β laths of different width nucleate and grow at different temperatures so that their compositions differ substantially. Fig. 10 presents such an example that finer β laths exhibit much higher V content than the coarser ones. The EDS point analysis (wt.%) indicated that β_1: 26.61 ± 2.08% V, 1.47 ± 0.28% Al, 3.31 ± 0.48% Fe; β_2: 13.96 ± 4.87% V, 3.17 ± 0.78% Al, 1.50 ± 0.64% Fe; β_3: 6.04 ± 0.52% V, 4.75 ± 0.07% Al, 0.43 ± 0.06% Fe. We can thus predict that finer β laths form at lower temperatures.

3.4. Columnar to equiaxed transition in SLM Ti-6Al-4V

During SLM processing, a temperature rise to 600–850 °C in the preceding solidified layers reduces cooling rate and results in heat build-up in the vicinity of the melt pool due to limited heat

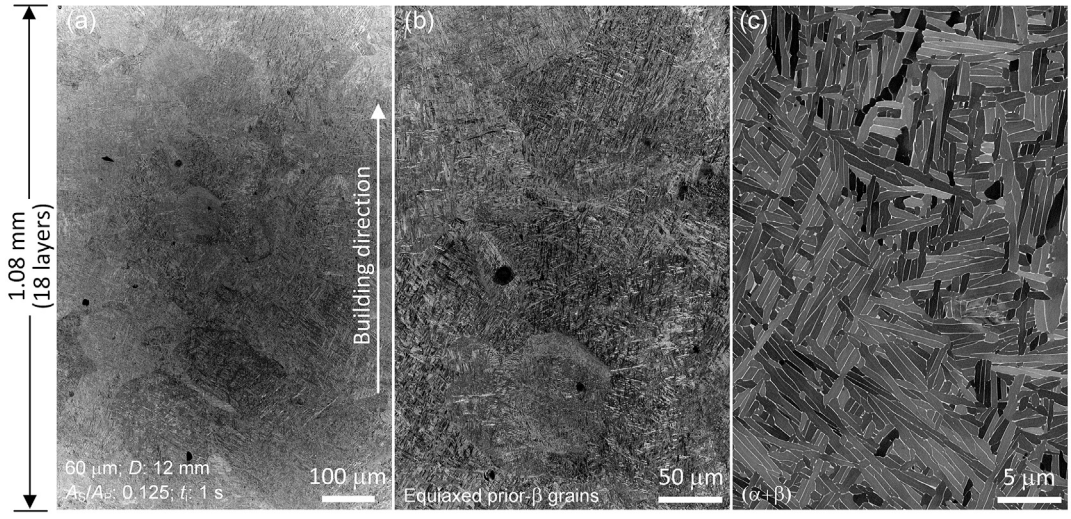

Fig. 11. Longitudinal section showing equiaxed prior-β grains of 50–200 μm present in SLM as-built Ti-6Al-4V ($A_S/A_P = 0.125$, $t_i = 1$ s, $t = 60$ μm). (a) Low magnification. In this micrograph, the total distance along the building direction is 1.08 mm, about 18 layers. (b) High magnification. (c) Equiaxed prior-β grains contain lamellar (α+β) instead of α′ martensite. Continuous α layer is absent at the boundary of prior-β grains.

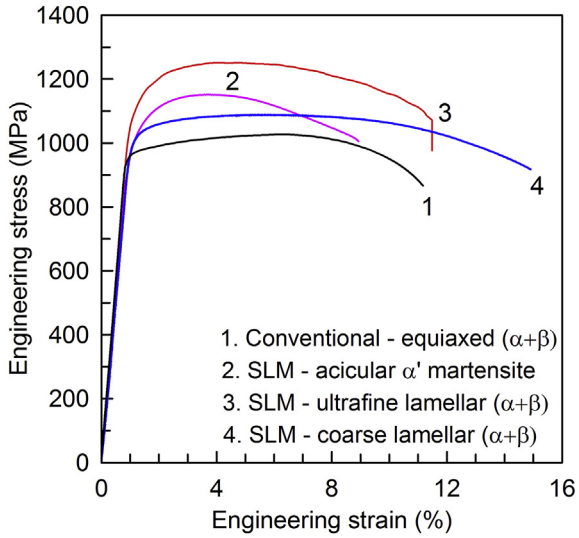

Fig. 12. Engineering tensile stress-strain curves of SLM as-built Ti-6Al-4V comprising α′ martensite, ultrafine lamellar (α+β), and coarse lamellar (α+β). Conventional mill-annealed Ti-6Al-4V with equiaxed (α+β) is present for comparison.

dissipation. This further leads to substantial reduction of temperature gradient within the melt pool of forming the subsequent layer. The direct consequence of reduced temperature gradient is a possible transition from columnar to equiaxed grains (CET) [23]. A typical example shown in Fig. 11 clearly presents the production of equiaxed prior-β grains of 50–200 μm in one SLM as-built Ti-6Al-4V that experiences significant *in-situ* α′ martensite decomposition. Note that the commonly viewed α′ martensite was completely replaced by a fine lamellar (α+β) with α lath width of 0.59 ± 0.21 μm and β lath width of 63 ± 32 nm (Fig. 11c). Furthermore, the absence of continuous grain boundary α makes the lamellar (α+β) microstructure more crack resistant when subjected to mechanical load.

3.5. Mechanical performance of AM Ti-6Al-4V

The unfavoured microstructure of α′ martensite leads to inadequate ductility (total elongation to failure < 10%, e.g. curve 2 in Fig. 12) and low toughness (16–67 MPa$\sqrt{m}$), the major deficiencies of SLM as-built Ti-6Al-4V relative to its conventional or EBM as-built counterparts [6]. Transforming α′ martensite *in situ* into an ultrafine lamellar (α+β) microstructure has overcome the deficiency of poor mechanical performance to achieve both high strength and good ductility (curve 3 in Fig. 12) [8,14]. In this study, we further extend the capability to tailor microstructure *in situ* and produce equiaxed prior-β grains containing lamellar (α+β). The width of α laths is tuneable in a broad range of 0.15–0.8 μm. This achievement allows for the direct fabrication of Ti-6Al-4V by SLM with a broad range of mechanical properties. For example, a relatively coarse lamellar (α+β) microstructure in SLM as-built Ti-6Al-4V (Fig. 3c, $A_S/A_P = 0.4$, t_i = 1 s, 60 μm) resulted in an excellent combination of high strength (yield strength: 1022 ± 10 MPa; ultimate tensile strength: 1090 ± 10 MPa) and a decent elongation to failure up to 15% (curve 4 in Fig. 12). Even though the attained strength is slightly lower than that of the ultrafine lamellar (α+β) (curve 3 in Fig. 12), its uniform elongation of 7–8% that is comparable to that of the mill-annealed Ti-6Al-4V (curve 1 in Fig. 12), is much higher than 5% of the ultrafine lamellar (α+β) and 4% of the α′ martensite microstructure. Considering the effect of inter-layer time, in Fig. 13 and Table 2 we summarize tensile properties achieved in SLM as-built Ti-6Al-4V with a lamellar (α+β) microstructure produced using different inter-layer time (Group 2 in Table 1). Note that the achievable

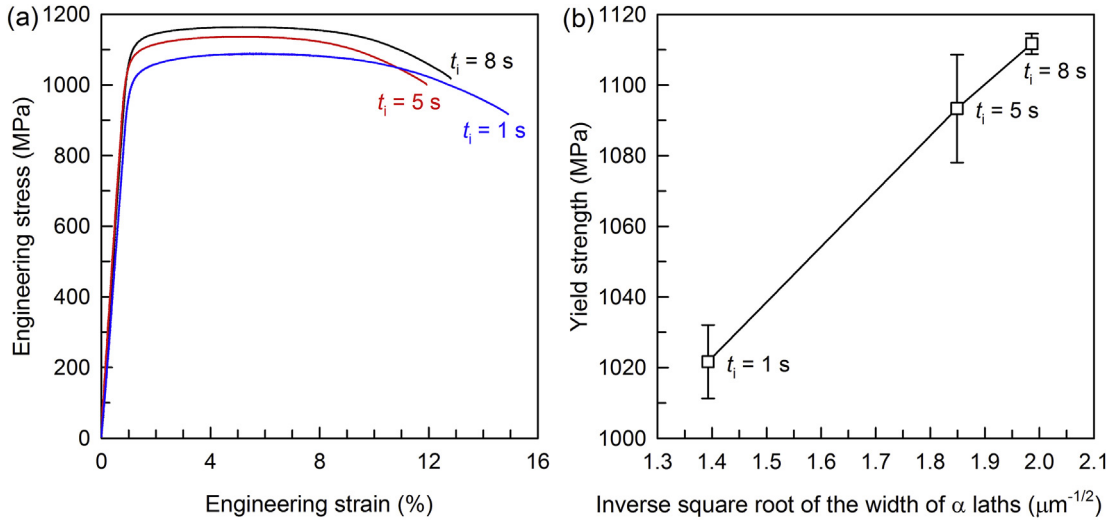

Fig. 13. (a) Engineering tensile stress-strain curves of SLM as-built Ti-6Al-4V with a lamellar (α+β) microstructure produced using different inter-layer time. (b) A Hall-Petch type relationship between yield strength and the width of α laths.

Table 2
Tensile properties of SLM as-built Ti-6Al-4V with a lamellar (α+β) microstructure produced using different inter-layer time ($A_S/A_P = 0.4$, t = 60 μm, D = 12 mm).

Inter-layer time t_i (s)	Width of α lath L_α (μm)	Yield strength $\sigma_{0.2}$ (MPa)	Ultimate tensile strength σ_{UTS} (MPa)	Elongation to failure EL (%)
1	0.52 ± 0.22	1022 ± 10	1090 ± 10	12.7 ± 2.1
5	0.29 ± 0.13	1093 ± 15	1149 ± 11	11.3 ± 0.5
8	0.25 ± 0.10	1112 ± 3	1165 ± 2	11.6 ± 1.2

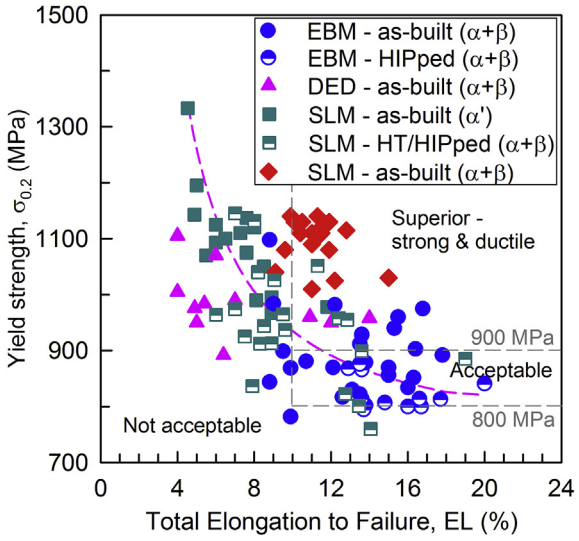

Fig. 14. Yield strength vs. total elongation to failure for Ti-6Al-4V fabricated by different AM methods. The curve of best fit excludes data on SLM as-built Ti-6Al-4V with lamellar (α+β) microstructure. Data for the as-built EBM, HIPped EBM, as-built SLM (α′) and as-built DED Ti-6Al-4V were obtained from Refs. [6,18,25]. Data for post heat treated/stress relieved SLM Ti-6Al-4V and HIPped SLM Ti-6Al-4V were adopted from Refs. [5,6,9].

yield strength is relevant to the width of α laths and its dependency is analogous to the Hall-Petch relationship [24]. All three lamellar (α+β) microstructures result in a total elongation to failure above 11%, but the microstructure containing coarser α laths in the case of 1 s leads to an elongation of 12.7 ± 2.1% which has never been achieved in SLM as-built Ti-6Al-4V.

Based on tensile property data available in the literature [5,6,9,18,25], we present in Fig. 14 a comparison of yield strength vs. total elongation to failure for the as-built Ti-6Al-4V made by both PBF (SLM, EBM) and direct energy deposition (DED) processes, post heat treated/stress relieved SLM Ti-6Al-4V, EBM Ti-6Al-4V post-treated by hot isostatic pressing (HIP), and HIPped SLM Ti-6Al-4V. Tensile data of total elongation less than 4% are excluded as such low ductility is primarily caused by the presence of defects such as lack of fusions and porosity. Relative to its EBM as-built counterparts, SLM as-built Ti-6Al-4V with α′ martensite exhibits higher strength but noticeably lower ductility. Post heat treatment and HIP processing greatly improves ductility of SLM Ti-6Al-4V at the expense of strength [5,6,9,26] but it has marginal effect on EBM Ti-6Al-4V [18]. This is not surprising because for SLM as-built Ti-6Al-4V HIP (usually at 920 °C with a pressure of 100 MPa) not only eliminates the defects such as porosity and lack of fusions but also transforms α′ martensite into lamellar (α+β). While for EBM as-built Ti-6Al-4V, the major role of HIP is for defect elimination even though the coarsening of the lamellar microstructure takes place at the same time. Ti-6Al-4V built by DED has shown a high degree of data scatter of tensile properties but the majority fall into the regime of low ductility with moderate strength. In contrast, the creation of lamellar (α+β) microstructure in SLM as-built Ti-6Al-4V overcomes the deficiency of α′ martensite and offers mechanical performance well exceeding ASTM standards (ELI Ti-6Al-4V, ASTM F136-13, F3001-14). According to the standards, here we artificially set the performance of minimum 10% elongation with yield strength of 800–900 MPa as “acceptable” while above 900 MPa as “superior”. Note that the mechanical performance of our newly developed SLM Ti-6Al-4V with lamellar (α+β) microstructure outperforms the majority of EBM and DED as-built Ti-6Al-4V.

4. Conclusions

In summary, our results show that

- A proper combination of SLM processing variables can enable significant *in situ* α′ martensite decomposition to produce a series of lamellar (α+β) microstructures whose characteristic length scale can be tuned from 0.15 to 0.8 μm. From the range of processing variables, the inter-layer time and layer thickness are more influential and decisive in promoting *in-situ* martensite decomposition. Shorter inter-layer time, larger layer thickness, less contact between support structure and part, and larger part dimension are in favour of martensite decomposition.
- As α′ martensite decomposition is diffusion-controlled, all characteristic features of the achieved lamellar (α+β) microstructures depend on transformation temperature and its residence time. More quantitatively, we find that the β phase has a lattice parameter in a specific range of 3.18–3.21 Å, which allows for a better prediction whether significant martensite decomposition takes place *in situ* in the duration of SLM processing.
- The V content in the β laths is another indicator of the occurrence of martensite decomposition. More specifically, the measured range of 5–25 wt% V corresponds to a temperature range of 600–850 °C at which the majority of the β laths form.
- Meanwhile, one of the direct consequences of the temperature rise (from the operating temperature of 200 °C to 600–850 °C) is the reduction of temperature gradient within the melt pool and equiaxed rather than columnar prior-β grains are thus favoured.
- A great combination of strength and ductility is achieved, thanks to the production of lamellar (α+β) contained in equiaxed prior-β grains. We expect that this study will have implications in the development of high performance Ti-6Al-4V by additive manufacturing.

Acknowledgements

This study is funded by the Australian Research Council through the Discovery Project Grant of DP150104719 and the Linkage Project Grant of LP140100607. The authors acknowledge the facilities, and the scientific and technical assistance, of the Australian Microscopy & Microanalysis Research Facility at RMIT University.

References

[1] L. Thijs, F. Verhaeghe, T. Craeghs, J. Van Humbeeck, J.P. Kruth, A study of the micro structural evolution during selective laser melting of Ti-6Al-4V, Acta Mater. 58 (2010) 3303–3312.
[2] W.J. Sames, F.A. List, S. Pannala, R.R. Dehoff, S.S. Babu, The metallurgy and processing science of metal additive manufacturing, Int. Mater. Rev. 61 (2016) 315–360.
[3] B. Vandenbroucke, J.P. Kruth, Selective laser melting of biocompatible metals for rapid manufacturing of medical parts, Rapid Prototyp. J. 13 (2007) 196–203.
[4] L. Facchini, E. Magalini, P. Robotti, A. Molinari, S. Hoges, K. Wissenbach, Ductility of a Ti-6Al-4V alloy produced by selective laser melting of prealloyed powders, Rapid Prototyp. J. 16 (2010) 450–459.
[5] T. Vilaro, C. Colin, J.D. Bartout, As-fabricated and heat-treated microstructures of the Ti-6Al-4V alloy processed by selective laser melting, Metall, Mater. Trans. A 42A (2011) 3190–3199.
[6] J.J. Lewandowski, M. Seifi, Metal additive manufacturing: a review of mechanical properties, Annu. Rev. Mater. Res. 46 (2016) 151–186.
[7] P. Li, D.H. Warner, A. Fatemi, N. Phan, Critical assessment of the fatigue performance of additively manufactured Ti-6Al-4V and perspective for future research, Int. J. Fatigue 85 (2016) 130–143.
[8] W. Xu, M. Brandt, S. Sun, J. Elambasseril, Q. Liu, K. Latham, K. Xia, M. Qian, Additive manufacturing of strong and ductile Ti-6Al-4V by selective laser melting via in-situ martensite decomposition, Acta Mater. 85 (2015) 74–84.
[9] B. Vrancken, L. Thijs, J.P. Kruth, J. Van Humbeeck, Heat treatment of Ti6Al4V produced by selective laser melting: microstructure and mechanical properties, J. Alloy. Compd. 541 (2012) 177–185.

[10] P.C. Collins, D.A. Brice, P. Samimi, I. Ghamarian, H.L. Fraser, Microstructural control of additively manufactured metallic materials, Annu. Rev. Mater. Res. 46 (2016) 63–91.
[11] M. Simonelli, Y.Y. Tse, C. Tuck, On the texture formation of selective laser melted Ti-6Al-4V, Metall. Mater. Trans. A 45A (2014) 2863–2872.
[12] M. Qian, W. Xu, M. Brandt, H.P. Tang, Additive manufacturing and post-processing of Ti-6Al-4V for superior mechanical properties, MRS Bull. 41 (2016) 775–783.
[13] D. Herzog, V. Seyda, E. Wycisk, C. Emmelmann, Additive manufacturing of metals, Acta Mater. 117 (2016) 371–392.
[14] W. Xu, S. Sun, J. Elambasseril, Q. Liu, M. Brandt, M. Qian, Ti-6Al-4V additively manufactured by selective laser melting with superior mechanical properties, JOM 67 (2015) 668–673.
[15] G.J. Marshall, W.J. Young, S.M. Thompson, N. Shamsaei, S.R. Daniewicz, S. Shao, Understanding the microstructure formation of Ti-6Al-4V during direct laser deposition via in-situ thermal monitoring, JOM 68 (2016) 778–790.
[16] P.A. Kobryn, S.L. Semiatin, The laser additive manufacture of Ti-6Al-4V, JOM 53 (2001) 40–42.
[17] S.S. Al-Bermani, M.L. Blackmore, W. Zhang, I. Todd, The origin of microstructural diversity, texture, and mechanical properties in electron beam melted Ti-6Al-4V, Metall. Mater. Trans. A 41A (2010) 3422–3434.
[18] S.L. Lu, H.P. Tang, Y.P. Ning, N. Liu, D.H. Stjohn, M. Qian, Microstructure and mechanical properties of long Ti-6Al-4V rods additively manufactured by selective electron beam melting out of a deep powder bed and the effect of subsequent hot isostatic pressing, Metall, Mater. Trans. A 46A (2015) 3824–3834.
[19] F.X.G. Mur, D. Rodriguez, J.A. Planell, Influence of tempering temperature and time on the alpha'-Ti-6Al-4V martensite, J. Alloy. Compd. 234 (1996) 287–289.
[20] J.I. Qazi, O.N. Senkov, J. Rahim, F.H. Froes, Kinetics of martensite decomposition in Ti-6Al-4V-xH alloys, Mater. Sci. Eng. A 359 (2003) 137–149.
[21] R. Boyer, G. Welsch, E.W. Collings, Materials Properties Handbook: Titanium Alloys, ASM International, Materials Park, OH, 1994.
[22] J.W. Elmer, T.A. Palmer, S.S. Babu, E.D. Specht, In situ observations of lattice expansion and transformation rates of alpha and beta phases in Ti-6Al-4V, Mater. Sci. Eng. A 391 (2005) 104–113.
[23] J.A. Spittle, Columnar to equiaxed grain transition in as solidified alloys, Int. Mater. Rev. 51 (2006) 247–269.
[24] N. Hansen, Hall-Petch relation and boundary strengthening, Scr. Mater. 51 (2004) 801–806.
[25] H.P. Tang, M. Qian, N. Liu, X.Z. Zhang, G.Y. Yang, J. Wang, Effect of powder reuse times on additive manufacturing of Ti-6Al-4V by selective electron beam melting, JOM 67 (2015) 555–563.
[26] S. Leuders, T. Lieneke, S. Lammers, T. Troester, T. Niendorf, On the fatigue properties of metals manufactured by selective laser melting - the role of ductility, J. Mater. Res. 29 (2014) 1911–1919.
[27] A. Safdar, L.Y. Wei, A. Snis, Z. Lai, Evaluation of microstructural development in electron beam melted Ti-6Al-4V, Mater. Charact. 65 (2012) 8–15.
[28] L. Facchini, E. Magalini, P. Robotti, A. Molinari, Microstructure and mechanical properties of Ti-6Al-4V produced by electron beam melting of pre-alloyed powders, Rapid Prototyp. J. 15 (2009) 171–178.
[29] X. Tan, Y. Kok, Y.J. Tan, M. Descoins, D. Mangelinck, S.B. Tor, K.F. Leong, C.K. Chua, Graded microstructure and mechanical properties of additive manufactured Ti-6Al-4V via electron beam melting, Acta Mater. 97 (2015) 1–16.
[30] H.K. Rafi, N.V. Karthik, H.J. Gong, T.L. Starr, B.E. Stucker, Microstructures and mechanical properties of Ti6Al4V parts fabricated by selective laser melting and electron beam melting, J. Mater. Eng. Perform. 22 (2013) 3872–3883.